Nanoscale Horizons

ROYAL SOCIETY OF CHEMISTRY

COMMUNICATION

View Article Online
View Journal | View Issue

Cite this: *Nanoscale Horiz.*, 2025, 10, 2454

Received 29th March 2025,
Accepted 18th July 2025

DOI: 10.1039/d5nh00192g

rsc.li/nanoscale-horizons

Emergence of a zero-bias peak on the MgO/Fe(001) surface induced by the adsorption of a spin-1/2 molecule†

Kyosei Ishii,[a] Nana K. M. Nazriq,[a] Peter Krüger [ab] and Toyo Kazu Yamada *[ab]

Engineering electronically decoupled spin states is essential for achieving robust spin by suppressing inelastic spin-flip scattering induced by conduction electrons. Accordingly, the fabrication of spins on insulating ultrathin films such as MgO or NaCl deposited on metallic substrates has been intensively investigated over the past decades to mitigate electronic hybridization. However, these studies have predominantly focused on non-magnetic noble metal substrates. In this work, we experimentally demonstrate that ultrathin MgO films grown on a ferromagnetic Fe(001) substrate, commonly employed in tunnel magnetoresistance sensors, can serve as an advanced platform for realizing electronically isolated spin states. As a prototypical system, we utilize a copper (Cu) ion (S = 1/2) embedded within a copper-phthalocyanine (CuPc) molecule. An atomically flat and clean insulating surface is obtained by optimizing the epitaxial growth conditions of ~1 nm-thick MgO films on an Fe(001) whisker substrate precoated with a $p(1 \times 1)$ oxygen layer. Scanning tunneling microscopy (STM) conducted at 4.6 K under ultrahigh vacuum conditions shows individual CuPc molecules adsorbed on the MgO surface. Simultaneous scanning tunneling spectroscopy (STS) reveals a well-defined molecular energy gap. Remarkably, a pronounced zero-bias peak (ZBP) emerges within this gap, signifying the presence of an electronically isolated spin on the MgO/Fe(001) heterostructure. Moreover, STS measurements reveal the lateral extension of the ZBP across the insulating film. These findings pave the way for engineering isolated molecular spin states on ferromagnetic substrates, offering new possibilities for manipulating spin states through substrate-mediated magnetic interactions.

New concepts

Establishing robust isolated spins on solid surfaces through the epitaxial growth of two-dimensional films is crucial for the development of quantum spin-based technologies, such as qubits, quantum sensors, and single-atom catalysts. Traditionally, the zero-bias peak (ZBP), a hallmark of isolated spin states, has been extensively studied on noble metal surfaces. However, these surfaces are rich in conduction electrons, which can screen the spins and alter their intrinsic properties. In this study, we demonstrate that a Fe(001) ferromagnetic substrate can serve as an advanced platform for engineering isolated spins on solid surfaces. This was achieved by introducing an atomically flat insulating MgO layer between the spin and the substrate. By adsorbing a spin-1/2 molecule onto the MgO/Fe(001) surface, we observed the emergence of a ZBP within the energy gap. This discovery opens new avenues for tailoring quantum spin states using ferromagnetic substrates and highlights the MgO/Fe(001) system, already widely used in tunnel magnetoresistance sensors, as a promising platform for hosting isolated spins.

1. Introduction

Creating a robust isolated spin ($S \neq 0$) utilizing condensed matter materials is crucial for realizing quantum bits, sensors, and single-atom catalysts.[1–6] Therefore, over the past few decades, significant efforts have been dedicated to identifying materials capable of producing a stable quantum spin. Promising candidates include single transition-metal atoms,[7] molecular magnets,[8] nitrogen-vacancy centers in diamonds,[9–11] and two-dimensional (2D) layered materials.[12,13] One approach to accessing and confirming the presence of localized spins is by observing a zero-bias peak (ZBP). The ZBP may result from antiferromagnetic exchange coupling ($J < 0$) between the localized spin (a magnetic impurity) and conduction electrons on a noble metal surface,[14] recognized as the Kondo resonance.[15–41] In this study, a Cu(II) ion possessing an unpaired electron (S = 1/2) in the Cu-phthalocyanine molecule (CuPc): a planar conjugated molecule with a center Cu-ion, where nitrogen atoms connect four isoindole units (Fig. 1a, and Fig. S2 and S4, ESI†) is used as a standard test sample.[29,42,43]

To date, the engineering of these ZBPs has been primarily limited to noble metal surfaces, while the molecule–metal interactions in these systems could change the intrinsic nature of the molecular spins. Although the appearance of a ZBP can

[a] *Department of Materials Science, Chiba University, 1-33 Yayoi-cho, Inage-ku, Chiba 263-8522, Japan. E-mail: toyoyamada@faculty.chiba-u.jp*
[b] *Molecular Chirality Research Centre, Chiba University, 1-33 Yayoi-cho, Inage-ku, Chiba 263-8522, Japan*

† Electronic supplementary information (ESI) available. See DOI: https://doi.org/10.1039/d5nh00192g

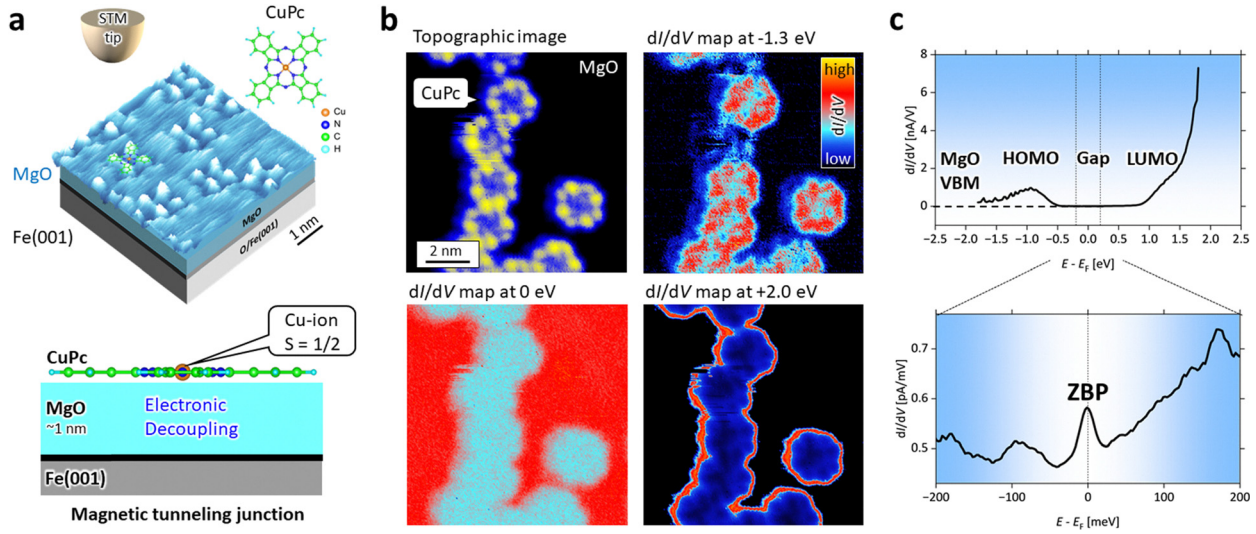

Fig. 1 (a) STM topographic image of the MgO/O/Fe(001) surface after CuPc deposition in a 3D view mode: (5 × 5 nm^2, V_s = +0.3 V, I_t = 500 pA). Lower panel: Schematic diagram of STM zero-bias peak (ZBP) measurement using a single molecular spin in an MTJ system. (b) STM topographic image (10 × 10 nm^2, V_s = −2.0 V, I_t = 50 pA) and simultaneously obtained d*I*/d*V* maps at −1.3 V, 0 V, and +2.0 V. (c) d*I*/d*V* spectra measured on a CuPc molecule.

indicate the localization of the spin, the inexhaustible conduction electrons on metal surfaces screen the spin and further alter it *via* the Ruderman–Kittel–Kasuya–Yosida (RKKY) interaction, leading to a short spin lifetime.

In order to cut the screening or spin scattering by the conduction electrons, the potential of insulating film surfaces, such as Al_2O_3,[44] MgO,[45] NaCl,[46,47] or CuN[48] on non-magnetic noble metal substrates has been examined. On the other hand, the absence of delocalized conduction electrons on these surfaces might lead to no ZBP appearance as *J* would be zero.

Here, we demonstrate the use of the MgO/Fe(001) system, commonly employed in tunnel magnetoresistance (TMR) devices,[49–51] to realize isolated spin states on an insulating solid surface. A distinctive feature of this system is the use of a ferromagnetic substrate. Crucially, however, the molecule is not in direct contact with the metal substrate but separated by the insulating MgO layers. Thereby, the strong interaction between metal-3d and molecular π-states, which may quench the molecular spin, is prevented. Indeed, direct adsorption of phthalocyanines on a transition metal substrate leads to the formation of chemical bonds involving the 3d surface states.[52–54] This behavior contrasts sharply with that observed on non-magnetic noble metal substrates.

However, if it can be experimentally demonstrated that isolated spins are preserved on the Fe(001) substrate by suppressing electronic hybridization through the insertion of insulating films, research on isolated spins on insulating solid surfaces could be significantly expanded beyond the current limitation to non-magnetic noble metal substrates, paving the way for the use of magnetic substrates that are widely employed in spintronic applications.

As a ferromagnetic substrate, we used an Fe(001) whisker single crystal grown *via* chemical vapor deposition, which has atomically flat terraces with terrace widths larger than 100 nm (impurity less than 1%).[54–57] The first difficult part of realizing this CuPc on MgO/Fe(001) was how to grow an atomically flat MgO surface on Fe(001) *via* epitaxial growth in an ultrahigh vacuum (UHV). Direct deposition of Mg in an oxygen atmosphere on Fe(001) provided a few-nanometer-sized MgO nanoclusters.[55] This was found to be due to the active Fe(001) during the growth, creating nucleation and restricting the thermal diffusion. Thus, we have developed the oxygen coating on the Fe(001), and the $p(1 \times 1)$-oxygen monolayer film coating provides an atomically-flat surface following the substrate Fe(001) atomic terraces (terrace width larger than 100 nm).[56] We found that MgO growth on this oxygen-precoating Fe(001) substrate generates an atomically flat MgO film (terrace width larger than 20 nm) with atomic defects less than 1%[55] (Fig. S1, ESI†).

Scanning tunneling microscopy (STM), conducted at 4.6 K in UHV, visualized individual CuPc molecules on the MgO/Fe(001) surface. Simultaneously obtained scanning tunneling spectroscopy (STS) measures the highest occupied molecular orbitals (HOMO) and the lowest unoccupied molecular orbitals (LUMO). Due to the absence of conduction electrons on the insulating MgO surface, the emergence of a ZBP is not expected. However, upon close examination near the Fermi energy (E_F) within the HOMO–LUMO gap, a ZBP was clearly observed. This finding suggests that electron-depleting insulating films can support the formation of isolated spins even on ferromagnetic substrates, not just on non-magnetic noble metals. Interestingly, the observed ZBP was found to spatially extend across the insulating MgO surface, a behavior not seen on noble metal substrates.

2. Experimental section

2.1 Home-built low-temperature UHV STM setup

STM measurements were performed using home-built UHV equipment consisting of STM, preparation, and deposition

chambers. The base pressures of each chamber were below 5.0×10^{-8} Pa, 2.0×10^{-8} Pa, and 1.0×10^{-7} Pa, respectively.[58–61] Samples and STM tips were transferred between chambers using transfer rods without breaking the UHV. Gate valves separated each chamber. A UHV cryostat (CryoVAC) in the STM chamber was used to cool down the STM stage. We used tungsten tips as STM probes, created using conventional chemical etching and flame etching, producing a sharp tip within 3 seconds.[62–65]

2.2 STM/STS measurements and ZBP fitting analysis

With the nanonis SPM controller BP4, STM measurements obtained topographic images of sample surfaces in constant current mode. The STM data were analyzed using WSxM 5.0 Develop 10.2 software[66] and Gwyddion 2.56. 3D differential conductance (dI/dV) maps (x-axis: distance [nm], y-axis: energy: $E - E_F$ [meV], and z-axis: dI/dV [pA mV^{-1}]) along a one-dimensional line on the sample were obtained using OriginPro2024.

We fitted the dI/dV data for quantitative analysis using the Fano equation and the Lorentzian function. The dI/dV signal is proportional to the Fano function:[28,67,68] $(q + \varepsilon)^2/(1 + \varepsilon^2)$, where $\varepsilon = (eV - E_c)/\Gamma$. Here, E_c represents the peak center position, q is the Fano parameter, and Γ represents the half-width-half-maximum (HWHM). In the limit of temperature $T \rightarrow 0$ K, $\Gamma \approx k_B T_K$,[33,69] where k_B is the Boltzmann constant, and T_K is the so-called Kondo temperature. This approximation allows for the extrapolation of T_K. For large values of q, the Fano peak approaches a Lorentzian peak. To further analyze the intramolecular interaction, we performed cumulative fitting in Fig. 2b and 3g, including the ZBP and the side peaks. Due to the significant q value obtained from the Fano fitting of the ZBP, the Lorentzian function was employed: $y = y_0 + (2Aw)/\{4\pi(x - x_c)^2 + w^2\}$. Here, y_0 represents the offset, A is the peak area, w is the full-width-half-maximum (FWHM), and x_c is the peak center position. The side peak was fitted with a Gaussian function: $y = y_0 + A\exp\{-4\ln(2)\ (x - x_c)^2/w^2\}/\{w(\pi/4\ln 2)^{1/2}\}$, where y_0, A, w, and x_c have the same definitions as above. The background was fitted with a double exponential decay function due to its proportionality to the dI/dV signal:[70–72] $y = y_0 + A_1\exp(-x/t_1) + A_2\exp(-x/t_2)$. Here, y_0 is the offset, A_1 and A_2 are the amplitude for the two exponential terms, and t_1 and t_2 are the time constant. We have attempted the fitting with two Fano functions (see Fig. S5, ESI†). All fitting processes have been carried out using OriginPro 2024.

2.3 Cleaning process of Fe(001) substrate

A Fe(001) single-crystal whisker, grown by chemical vapor deposition,[54,73] was cleaned through repeated cycles of Ar^+ sputtering (+0.8 kV, +0.80 μA) at 820 K. The surface cleanliness and morphology were confirmed by STM/STS measurements,

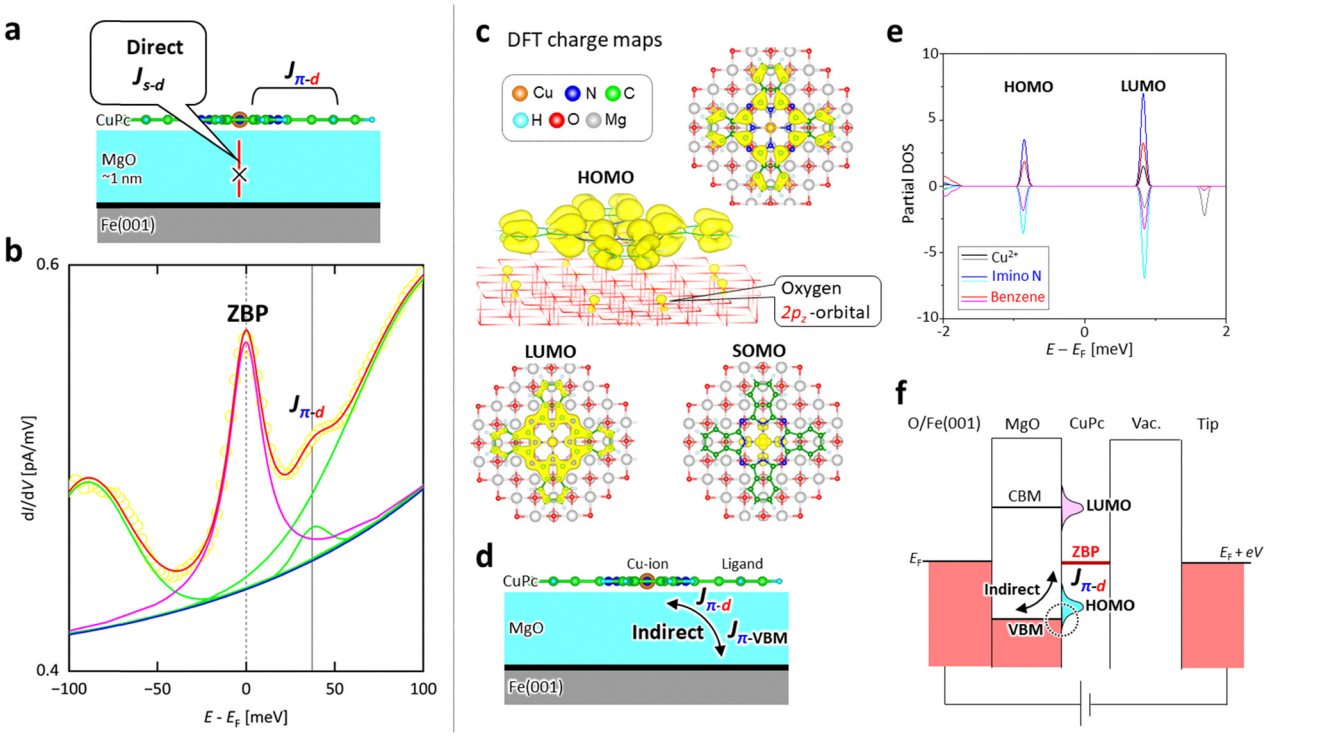

Fig. 2 (a) Cross-sectional view model of CuPc on MgO/O/Fe(001). Direct coupling: J_{s-d}. Blue and red arrows represent spin-exchange coupling. (b) Averaged dI/dV spectrum of CuPc (dots), with the cumulative fitted curve (orange line). The ZBP was fitted using a Lorentzian function (magenta line), while other peaks were fitted with Gaussian functions (green line). The fitting baseline is shown in blue. A reference line for $J_{\pi-d}$ is marked at 37 meV. (c) DFT charge maps at HOMO, LUMO, and SOMO levels. Top and side views are shown for the HOMO level. (d) Cross-section view model showing the indirect coupling through molecular ligands and MgO. (e) DFT partial DOS within CuPc. (f) Energy diagram depicting the double-barrier system between the W tip and Fe substrate, mediated by the CuPc molecule, with vacuum and MgO film as barriers. VBM and CBM denote the valence band maximum and conduction band minimum.

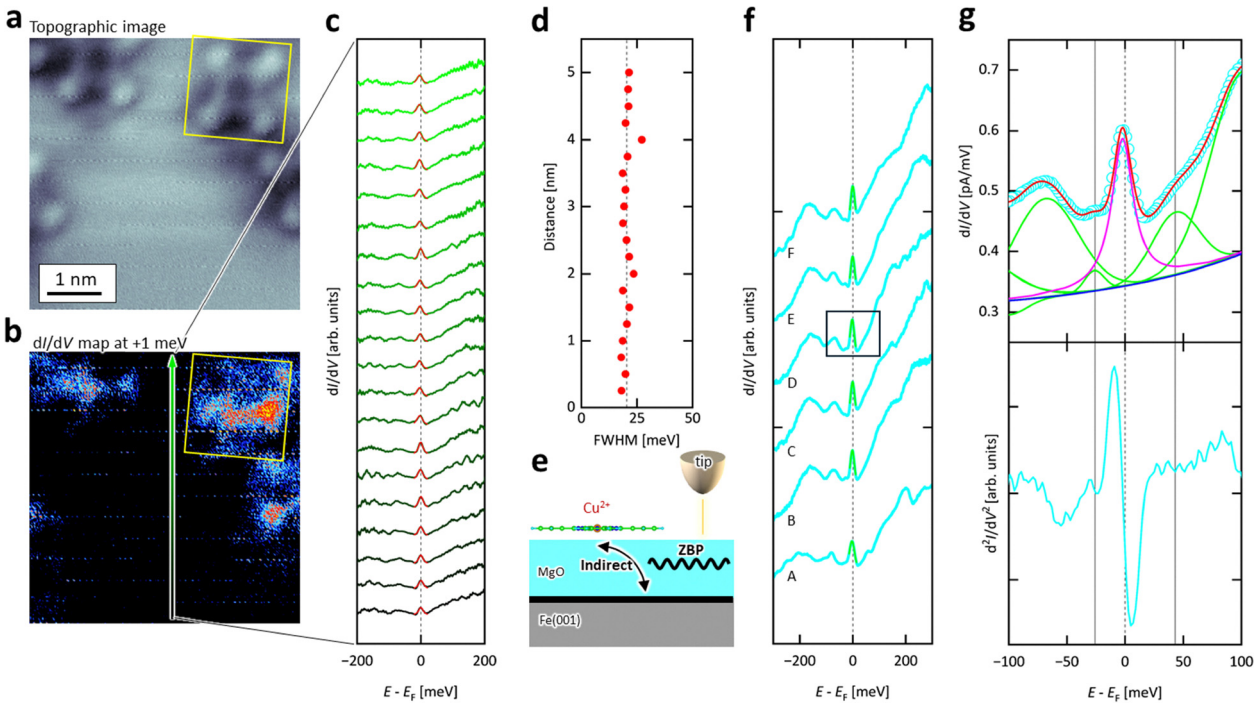

Fig. 3 (a) STM topographic image (5 × 5 nm^2, +0.5 V, 500 pA) and (b) d*I*/d*V* map (+1 mV) of CuPc on the MgO/O/Fe(001) surface, captured simultaneously. The boxes indicate the same CuPc molecule. (c) d*I*/d*V* spectra acquired along the green arrow in (b) from bottom to top. All ZBPs were fitted with Lorentzian functions, using the same number of data points for each fit. (d) The FWHM of the fitted curves from (c), with an average value of 20.4 meV, shown as a dotted line. (e) Cross-section view model showing the possible indirect super-exchange coupling through the CuPc ligands to the metal substrate and coherent ZBP propagation through the MgO film. (f) d*I*/d*V* spectra (sky-blue, labeled A–F) obtained on the MgO surface at different times, with the ZBP fitted using Lorentzian functions (green). (g) Upper panel: d*I*/d*V* spectrum from spectrum D in (f), where the experimental data (sky-blue) was fitted (red line) using a Lorentzian (magenta line) combined with Gaussians (green lines) and a baseline (blue line). Lower panel: d^2I/dV^2 spectrum. Two lines mark energy positions of −26 meV and +43 meV.

which revealed atomically flat terraces with widths of 50–100 nm and a characteristic Fe(001) 3d surface state peak at +0.2 eV in the d*I*/d*V* spectra.[54,74–77] Low-energy electron diffraction (LEED) patterns exhibited the four-fold symmetry characteristic of the bcc(001) surface.

2.4 Oxygen-precoating process on Fe(001)

The Fe(001)–$p(1 \times 1)$O surface was prepared in the preparation chamber by exposing the clean Fe(001) surface to oxygen gas at a pressure of approximately 4×10^{-6} Pa for 60 seconds (equivalent to 2 Langmuir), while maintaining the substrate temperature at 300 K. The sample was then annealed at 850 K for 15 minutes. STM topographic imaging revealed a well-defined $p(1 \times 1)$ structure, in which the dark spots correspond to the positions of oxygen atoms.[56,78,79] This monolayer oxygen coating serves to prevent further oxidation and interfacial roughening.

2.5 Ultrathin MgO film growth on Fe(001)–$p(1 \times 1)$O

The Fe(001)–$p(1 \times 1)$O surface was further exposed to oxygen gas (60 s, 1×10^{-6} Pa) in the preparation chamber, followed by deposition of Mg atoms from an evaporator (AEV-3, AVC Co., Ltd) at a substrate temperature of 750 K. STM images revealed the formation of atomically flat, ultrathin, square-shaped nanoislands with terrace widths of approximately 40 nm and a uniform height of about 1 nm (see Fig. S1, ESI†). Terraces of the underlying Fe(001)–$p(1 \times 1)$O surface remained visible between the islands.[80] The areal density of MgO islands on the O/Fe(001) substrate remains approximately 0.0005 nm^{-2}, corresponding to roughly five islands within a 100×100 nm^2 area.

2.6 CuPc adsorption

CuPc molecules were deposited onto this MgO surface in the deposition chamber with single-molecule-level control using a quartz crystal microbalance (QCM)[81] (Fig. S3, ESI†). The CuPc source was loaded into the evaporator's crucible and degassed for 3 hours. Before CuPc deposition, the MgO/Fe(001)–$p(1 \times 1)$O sample was cooled to cryogenic temperature by placing it on the 5 K STM stage. The sample was gently transferred to the preparation chamber within a few minutes, and CuPc was deposited within 3 to 5 seconds. During the deposition, the crucible temperature was set to 553 K (filament current: 3.6 A), and the chamber pressure remained at 3×10^{-7} Pa. It should be noted that CuPc deposition was performed within a few minutes after removing the sample from a 4.5 K cryostat. Therefore, the actual sample temperature during deposition was likely much lower than 300 K. Following deposition, the sample was immediately returned to the cryostat. This temperature condition may have limited the thermal diffusion of

CuPc molecules on the surface, resulting in the observation of isolated single CuPc molecules rather than a self-assembled monolayer (SAM) film. These results suggest that CuPc deposition at 300 K on MgO/O/Fe(001) would likely yield a SAM structure, due to the relatively weak CuPc–MgO interaction. CuPc single molecules were deposited on the surface with a density of approximately five molecules per 10×10 nm^2 area, in order to ensure isolation of individual CuPc molecules.

2.7 DFT calculation

Density functional theory (DFT) calculations of CuPc molecules on MgO were performed using the projector-augmented wave method as implemented in the VASP package.[82,83] The CuPc/MgO system was modelled with a MgO substrate of two atomic layers. The geometric structure was optimized using the PBE exchange–correlation functional together with Grimme's DFT-D3 van der Waals corrections. The electronic structure was then recalculated with the hybrid HSE06 functional,[84,85] which performs better than PBE for insulators and molecules.[86] The computational method is exactly the same as in ref. 55, where further details can be found.

3. Results and discussion

Since the MgO/Fe(001) system has been extensively used as a tunnel magnetoresistance (TMR) sensor due to its high spin-valve effect, significantly increasing the TMR ratio at 300 K.[49–51] However, achieving epitaxial growth of MgO films directly on Fe(001) is challenging, often resulting in the formation of MgO nanoislands instead of an atomically flat MgO surface. Recently, it was discovered that oxygen precoating on Fe(001), which forms a $p(1 \times 1)$ oxygen-ordered monolayer, enables the growth of a high-quality, atomically flat MgO surface with an atomic terrace width of $\sim$40 nm on Fe(001) (Fig. S1, ESI†).[55] This MgO surface has a band gap of approximately 3 eV, ranging from -2.0 (= valence band maximum: VBM) to +0.9 eV (= conduction band minimum: CBM) around E_F, making it suitable as an electronically decoupling layer from the metallic Fe substrate. Also, this decoupling could prolong the spin lifetime within the adsorbed magnetic atoms or ions, as the MgO(001) surface has been reported to create a single-atom permanent magnet.[45] This suggests that electronic decoupling from the substrate conduction electrons is essential for realizing a robust spin on a surface.

Fig. 1a–c show the experimental STM/STS results. We used metallic W tips, which were cleaned in UHV by electron bombardment, to prevent the formation of an oxygen layer on the W tip apex.[63,65] The tip was carefully approached to the surface with a setpoint sample bias exceeding the band gap energy, specifically with $V_s > 1$ V and $V_s < -2$ V.

Fig. 1a provides an STM topographic image obtained from the MgO surface with some clover-shaped CuPc single molecule adsorption, where a tip model illustrates how the STM tip could scan the surface. The MgO film has an approximately 3 eV wide insulating band gap, thus enabling the visualization of the adsorbed materials' intrinsic electronic characteristics by mitigating the substrate electronic interaction from Fe(001) (lower panel cross sectional model in Fig. 1a). Fig. 1b shows an STM topographic image and simultaneously obtained STS differential conductance (dI/dV) maps at -1.3, 0.0, and +2.0 V, where dI/dV is proportional to the sample LDOS, which correspond to HOMO, E_F, and LUMO of CuPc, showing different symmetry and spatial distribution, with shapes and features comparable to those observed on other insulating surfaces, such as CuPc/NaCl/Ag(111).[44,47,87]

Fig. 1c presents an example of measuring dI/dV curves on CuPc molecules on MgO/Fe(001). HOMO and LUMO peaks are visible, while no LDOS features are observable in the HOMO–LUMO gap, where the dI/dV values approach zero nA V^{-1}, while this seems to be normal as no conduction electrons on the insulating MgO surface. These STS data in Fig. 1b and c indicate that the MgO/Fe(001) surface can serve as an advanced platform for visualizing the intrinsic molecular orbitals of the CuPc HOMO and LUMO, as it provides electronic decoupling functionality.

Initially, we did not expect the presence of ZBP on the MgO surface since no conduction electrons near E_F. However, we found in the dI/dV map at 0.0 V in Fig. 1b, where the positions of CuPc appear in a different color from the surrounding MgO surface, indicating a variation in LDOS even within the gap. Then, we magnified the dI/dV curve around E_F, as depicted in the lower panel of Fig. 1c, and subsequently identified the ZBP around E_F.

The emerging ZBP of CuPc on MgO/Fe(001) could serve as direct evidence of the presence of an isolated spin even on the ferromagnetic Fe(001) substrate by inserting MgO films. More importantly, the meaning of the ZBP emergence on the MgO/Fe(001) surface indicates that there is still an access route to the CuPc spin *via* the ZBP in spite of the absence of conduction electrons on the insulating MgO surface.

However, a question remains as to why this ZBP appeared on the insulating surface, given the lack of direct s–d coupling between the Cu 3d orbital and the substrate's s-conduction band ($J_{s\text{–}d}$ in Fig. 2a). There are two possible explanations.

First, the insulating system might resemble the ZBP observed in CuPc/Ag(001), namely, the physisorbed molecular spin on a noble metal surface,[40] where Kondo resonance was observed,[43] since both cases can be categorized as a double barrier system made of a tip/vacuum/molecule/separation/metal-substrate. Therefore, the main ZBP accompanied by phonon-assisted satellite peaks appearance could be similar to the case of a radical molecular spin on a noble metal.[40] The clear difference between these systems is the "separation". For the molecular spin physisorbed on a noble metal surface, the separation is of the order of 200 pm, while for the CuPc on 4 MLs MgO/Fe(001), the separation increases to approximately 1000 pm. This increased distance could drastically reduce the number of tunneling electrons, following the exponential decay exp $(-2\kappa z)$, $\kappa \sim 1$ Å^{-1}: decay constant, z: separation (Å). The significantly larger separation, approximately five times greater, between the CuPc and the substrate's s-conduction

bands should markedly reduce the direct s–d interaction (Fig. 2a).

Despite this, we observed the ZBP, as shown in Fig. 1c. Therefore, there must be another route. The hint could be given by the emergence of the side peak at +37 meV, marked by $J_{\pi-d}$ in Fig. 2b. If the Cu-ion spin interacts with the π-orbital at the benzene ring, this could produce intramolecular exchange π–d coupling ($J_{\pi-d}$),[43] manifesting in the dI/dV spectra as a small peak or shoulder since the $J_{\pi-d}$ is a relatively weak interaction (Fig. S6, ESI†). An interesting point is that this energy position agrees with the $J_{\pi-d}$ peak at +36 meV found in the CuPc/Ag(001) system.[43] Therefore, $J_{\pi-d}$ may serve as a potential pathway for linking the Cu-ion spin to the molecular ligand.

To gain deeper insight into the system, we performed DFT calculations. Fig. 2c illustrates the calculated charge maps of CuPc at HOMO, LUMO, and singly occupied molecular orbital (SOMO) energies, placed on a bilayer MgO film with a bandgap of ∼3 eV, including no Fe(001) substrate. This DFT result does not show any surprising features, and the DOS of CuPc on MgO looks similar to that of gas-phase CuPc. However, this finding suggests a possible coupling mechanism between the Cu-ion spin and the substrate's s-electrons. As shown experimentally in Fig. 1c, the tail of the broad CuPc HOMO peak extends toward the VBM of MgO. This is supported by the non-zero dI/dV values observed in the energy range between −1 and −2 eV, indicating the presence of electronic hybridization. Such hybridization may act as an indirect pathway between molecule and substrate. In this content, we note that the side-view DFT charge map at the HOMO level in Fig. 2c shows the appearance of oxygen 2p$_z$ orbitals on the MgO surface, which could weakly hybridize with the molecular ligand orbitals that are far from the molecular center but below the sides of the benzene rings. The cross-sectional model depicted in Fig. 2d illustrates a plausible coupling route between the Cu spin and the s-conduction electrons of the substrate *via* exchange coupling through the ligands. The partial density of states for the Cu ion, imino nitrogen (N) atoms, and benzene ring positions within the CuPc molecule are presented in Fig. 2e, showing that the HOMO is a strongly hybridized state containing contributions from Cu 3d, benzene, and imino-N. As seen in Fig. 2c, imino-N and benzene groups interact with O-p$_z$ states of the MgO surface and thus may build a bridge for the super-exchange interaction between the molecular spin active Cu-3d states and the substrate *via* the valence band of the MgO layer. We also conducted a detailed analysis of the ZBP characteristics in three distinct regions of the CuPc molecule, the central Cu ion, the imino N atoms, and the benzene rings (see Supplementary Note, ESI†), and confirmed that the ZBP features within CuPc are comparable to those observed for CuPc adsorbed on noble metal substrates.[41] Fig. 2f illustrates the energy diagram for a possible indirect pathway through which the Cu-ion spin may couple with the substrate electrons, leading to the appearance of the ZBP within the gap.

Another interesting point of the ZBP on this MgO/Fe(001) surface is that the ZBP originating from the Cu-ion spin was observed not only within the CuPc but also on the insulating MgO surface. This observation, extending beyond the CuPc, stands in clear contrast to its behavior of CuPc on noble metal surfaces, where the high density of conduction electrons on the noble metals screens the ZBP within the CuPc. Fig. 3a and b present an STM topographic image and an STS dI/dV map at +1 mV, respectively, both obtained simultaneously from the same region. In Fig. 3a, four CuPc molecules are visible, with one highlighted by a box. The corresponding CuPc molecule is similarly marked in the dI/dV map (Fig. 3b), allowing for identification of the CuPc positions. Due to variations in the ZBP within the CuPc (see Supplementary Note, ESI†), the imino-N atom positions appear brighter, with higher ZBP amplitude, while the benzene rings appear darker, with lower ZBP amplitude. Surprisingly, when examining the ZBP on the MgO surface, a distinct feature was observed. Following the green arrow in the dI/dV map in Fig. 3b, we compared the ZBP in the dI/dV curves at each position (shown in Fig. 3c and their fitting parameters in Table S2, ESI†), and the FWHM was determined through fitting and summarized in Fig. 3d. The data in Fig. 3c and d are particularly intriguing, as the ZBP appears uniformly along the arrowed direction across the MgO surface in Fig. 3b. Initially, we expected the ZBP to decay with increasing distance from the Cu-ion spin; however, this expectation was incorrect. The experimental data in Fig. 3c and d indicate that the ZBP could remain consistent across the MgO surface. On the other hand, the ZBP appearance outside the CuPc on the insulating MgO surface is plausible, given that the screening length of the ZBP has been reported to extend over the micrometer scale in nano-scale junction measurements.[88] Thus, the emerging ZBP from the Cu-ion spin could propagate through the insulating MgO surface, as there are no conduction electrons near E_F to screen it.

For further insights into the ZBP on the MgO surface, we have also examined the specifics of the ZBP observed on the MgO surface to determine how the characteristics of the ZBP might differ from those within CuPc. Fig. 3f depicts dI/dV spectra acquired from six distinct positions on the MgO surface (Fig. S6 and Table S3, ESI†), revealing several satellite peaks adjacent to the ZBP within the MgO band gap. Fig. 3g illustrates the cumulative fitting results of the spectrum "E" in Fig. 3f, where we identified an extra sub-peak at +43 meV, closely aligned with the $J_{\pi-d}$ peak observed in CuPc at +37 meV in Fig. 2b, but also another sub-peak at −26 meV, where the dI/dV spectra with fitting curves (upper panel) and the second derivative d^2I/dV^2 spectra (lower panel) suggest inelastic scattering. This peak may correspond to magnon excitation in the Fe/MgO system around ±23 meV, as previously documented for the Fe/MgO/Fe system.[89]

Thus, as shown in Fig. 1–3, we observed the emergence of a ZBP on the MgO/Fe(001) surface, indicating the presence of an isolated spin that is electronically decoupled from direct hybridization with the metallic substrate. However, we were unable to determine whether the quantum axis of the spin-1/2 molecular state is pinned at 4.6 K, since the present measurements were conducted using non-magnetic tungsten tips. This suggests that the Cu ion spin may remain in a paramagnetic state.

Potential contributions to spin pinning could arise from local crystal fields induced by the MgO lattice,[45,90] or from magnetic exchange interactions transmitted through the MgO layers[91,92] from the Fe(001) whisker substrate, which possesses an in-plane magnetic easy axis.[54]

These considerations suggest a compelling direction for future research: exploring spin-switching dynamics and spin-state lifetimes using spin-polarized STM[53,57] and STM-based electron spin resonance (ESR) techniques.[93–95] Moreover, it would be valuable to investigate macroscopic spin characteristics, as CuPc single molecules may undergo thermal diffusion on the MgO surface, potentially resulting in the formation of a 2D SAM film. This, in turn, could facilitate the application of surface-averaged spectroscopic techniques, such as X-ray magnetic circular dichroism (XMCD),[96–98] to further elucidate the spin properties of the Cu ions.

4. Conclusions

Developing engineering methods to stabilize robust isolated spins on solid surfaces through the epitaxial growth of 2D films is crucial for advancing molecular spin-based devices, including qubits, quantum sensors, and single-atom catalysts. To achieve this goal, engineering the electronic isolation of spins on solid surfaces is essential for prolonging spin lifetime and enhancing thermal stability.

In this study, we demonstrate the formation of isolated spins on an atomically flat MgO surface, prepared on an oxygen-precoated Fe(001) whisker ferromagnetic substrate. CuPc was chosen as a standard test sample, as the Cu-ion has a spin of $S = 1/2$. The ~1 nm thick MgO film, which is electronically decoupled from Fe(001), provides a well-defined HOMO–LUMO gap.

Notably, a ZBP was observed within this gap, despite the electron-depleting nature of the surface near E_F. This observation suggests that the ZBP emerges *via* an indirect coupling between the Cu-ion spin and the conduction electrons in the Fe substrate, mediated by the MgO valence band and the CuPc ligand. Furthermore, due to the absence of conduction electrons on the MgO surface, the ZBP was also detected on the MgO surface outside the CuPc. Given that the MgO/Fe(001) system is widely used in TMR sensors, our findings provide important insights into the potential of leveraging spintronic materials to extend the formation of isolated spins for applications in quantum devices.

Author contributions

T. K. Y. conceived and designed the project. N. K. M. N. and T. K. Y. performed all STM/STS experiments. K. I. and N. K. M. N. analyzed all the data. P. K. performed all DFT calculations. K. I. and T. K. Y. wrote the first draft, and all authors corrected and added a discussion to the manuscript.

Conflicts of interest

There are no conflicts to declare.

Data availability

The data that support the findings of this study are available from the corresponding author, Toyo Kazu Yamada, upon reasonable request.

Acknowledgements

This work was supported by JSPS KAKENHI Grant Number 23H02033, the Murata Science Foundation, the Shorai Foundation for Science and Technology, the TEPCO Memorial Foundation, the Casio Science Promotion Foundation, and the Toshiaki Ogasawara Memorial Foundation. We thank Dr Eiichi Inami (Kochi University of Technology) and Dr Masaki Horie (Hokkaido University) for the fruitful discussion to improve the manuscript.

References

1 H.-K. Lo and H. F. Chau, Is Quantum Bit Commitment Really Possible?, *Phys. Rev. Lett.*, 1997, **78**(17), 3410–3413, DOI: **10.1103/PhysRevLett.78.3410**.
2 P. C. Maurer, G. Kucsko, C. Latta, L. Jiang, N. Y. Yao, S. D. Bennett, F. Pastawski, D. Hunger, N. Chisholm, M. Markham, D. J. Twitchen, J. I. Cirac and M. D. Lukin, Room-Temperature Quantum Bit Memory Exceeding One Second, *Science*, 2012, **336**(6086), 1283–1286, DOI: **10.1126/science.1220513**.
3 N. K. Langford, R. B. Dalton, M. D. Harvey, J. L. O'Brien, G. J. Pryde, A. Gilchrist, S. D. Bartlett and A. G. White, Measuring Entangled Qutrits and Their Use for Quantum Bit Commitment, *Phys. Rev. Lett.*, 2004, **93**(5), 053601, DOI: **10.1103/PhysRevLett.93.053601**.
4 C. L. Degen, F. Reinhard and P. Cappellaro, Quantum Sensing, *Rev. Mod. Phys.*, 2017, **89**(3), 035002, DOI: **10.1103/RevModPhys.89.035002**.
5 C. Matea, T. Mocan, F. Tabaran, T. Pop, O. Mosteanu, C. Puia, C. Iancu and L. Mocan, Quantum Dots in Imaging, Drug Delivery and Sensor Applications, *Int. J. Nanomed.*, 2017, **12**, 5421–5431, DOI: **10.2147/IJN.S138624**.
6 Single Atom Catalysts Push the Boundaries of Heterogeneous Catalysis, *Nat. Commun.*, 2021, **12**(1), 5884, DOI: **10.1038/s41467-021-26130-0**.
7 F. D. Natterer, K. Yang, W. Paul, P. Willke, T. Choi, T. Greber, A. J. Heinrich and C. P. Lutz, Reading and Writing Single-Atom Magnets, *Nature*, 2017, **543**(7644), 226–228, DOI: **10.1038/nature21371**.
8 E. Moreno-Pineda and W. Wernsdorfer, Measuring Molecular Magnets for Quantum Technologies, *Nat. Rev. Phys.*, 2021, **3**(9), 645–659, DOI: **10.1038/s42254-021-00340-3**.
9 M. W. Doherty, N. B. Manson, P. Delaney, F. Jelezko, J. Wrachtrup and L. C. L. Hollenberg, The Nitrogen-Vacancy Colour Centre in Diamond, *Phys. Rep.*, 2013, **528**(1), 1–45, DOI: **10.1016/j.physrep.2013.02.001**.
10 R. Schirhagl, K. Chang, M. Loretz and C. L. Degen, Nitrogen-Vacancy Centers in Diamond: Nanoscale Sensors for Physics

and Biology, *Annu. Rev. Phys. Chem.*, 2014, **65**(1), 83–105, DOI: **10.1146/annurev-physchem-040513-103659**.

11 A. Ariyaratne, D. Bluvstein, B. A. Myers and A. C. B. Jayich, Nanoscale Electrical Conductivity Imaging Using a Nitrogen-Vacancy Center in Diamond, *Nat. Commun.*, 2018, **9**(1), 2406, DOI: **10.1038/s41467-018-04798-1**.

12 A. Brenneis, L. Gaudreau, M. Seifert, H. Karl, M. S. Brandt, H. Huebl, J. A. Garrido, F. H. L. Koppens and A. W. Holleitner, Ultrafast Electronic Readout of Diamond Nitrogen–Vacancy Centres Coupled to Graphene, *Nat. Nanotechnol.*, 2015, **10**(2), 135–139, DOI: **10.1038/nnano.2014.276**.

13 F. Casola, T. Van Der Sar and A. Yacoby, Probing Condensed Matter Physics with Magnetometry Based on Nitrogen-Vacancy Centres in Diamond, *Nat. Rev. Mater.*, 2018, **3**(1), 17088, DOI: **10.1038/natrevmats.2017.88**.

14 P. A. Nozi, *"Fermi-Liquid" Description of the Kondo Problem at Low Temperatures*, 12.

15 N. Kumar, Y.-S. Lan, I. Jang, Y.-H. Lin, C.-J. Chen, T.-H. Lin, H.-T. Jeng, P.-Y. Chang and P.-J. Hsu, Atomic-Scale Magnetic Doping of Monolayer Stanene by Revealing Kondo Effect from Self-Assembled Fe Spin Entities, *npj Quantum Mater.*, 2024, **9**(1), 37, DOI: **10.1038/s41535-024-00647-1**.

16 F. Ara, S. M. Fakruddin Shahed, M. I. Hossain, K. Katoh, M. Yamashita and T. Komeda, Control of the Magnetic Interaction between Single-Molecule Magnet $TbPc_2$ and Superconductor $NbSe_2$ Surface by an Intercalated Co Atom, *Nano Lett.*, 2023, **23**(15), 6900–6906, DOI: **10.1021/acs.nanolett.3c01298**.

17 V. Vaňo, M. Amini, S. C. Ganguli, G. Chen, J. L. Lado, S. Kezilebieke and P. Liljeroth, Artificial Heavy Fermions in a van der Waals Heterostructure, *Nature*, 2021, **599**(7886), 582–586, DOI: **10.1038/s41586-021-04021-0**.

18 A. Zhao, Q. Li, L. Chen, H. Xiang, W. Wang, S. Pan, B. Wang, X. Xiao, J. Yang, J. G. Hou and Q. Zhu, Controlling the Kondo Effect of an Adsorbed Magnetic Ion Through Its Chemical Bonding, *Science*, 2005, **309**(5740), 1542–1544, DOI: **10.1126/science.1113449**.

19 P. Wahl, P. Simon, L. Diekhöner, V. S. Stepanyuk, P. Bruno, M. A. Schneider and K. Kern, Exchange Interaction between Single Magnetic Adatoms, *Phys. Rev. Lett.*, 2007, **98**(5), 056601, DOI: **10.1103/PhysRevLett.98.056601**.

20 A. Spinelli, M. Gerrits, R. Toskovic, B. Bryant, M. Ternes and A. F. Otte, Exploring the Phase Diagram of the Two-Impurity Kondo Problem, *Nat. Commun.*, 2015, **6**(1), 10046, DOI: **10.1038/ncomms10046**.

21 H. Prüser, P. E. Dargel, M. Bouhassoune, R. G. Ulbrich, T. Pruschke, S. Lounis and M. Wenderoth, Interplay between the Kondo Effect and the Ruderman–Kittel–Kasuya–Yosida Interaction, *Nat. Commun.*, 2014, **5**(1), 5417, DOI: **10.1038/ncomms6417**.

22 A. Zhao, Z. Hu, B. Wang, X. Xiao, J. Yang and J. G. Hou, Kondo Effect in Single Cobalt Phthalocyanine Molecules Adsorbed on Au(111) Monoatomic Steps, *J. Chem. Phys.*, 2008, **128**(23), 234705, DOI: **10.1063/1.2940338**.

23 N. Knorr, M. A. Schneider, L. Diekhöner, P. Wahl and K. Kern, Kondo Effect of Single Co Adatoms on Cu Surfaces, *Phys. Rev. Lett.*, 2002, **88**(9), 096804, DOI: **10.1103/PhysRevLett.88.096804**.

24 S. Meierott, N. Néel and J. Kröger, Kondo Effect of Single Co Atoms on Au(110), *Phys. Rev. B:Condens. Matter Mater. Phys.*, 2015, **91**(20), 201111, DOI: **10.1103/PhysRevB.91.201111**.

25 C. Van Efferen, J. Fischer, T. A. Costi, A. Rosch, T. Michely and W. Jolie, Modulated Kondo Screening along Magnetic Mirror Twin Boundaries in Monolayer MoS2, *Nat. Phys.*, 2024, **20**, 82–87, DOI: **10.1038/s41567-023-02250-w**.

26 Q. Zhang, W.-Y. He, Y. Zhang, Y. Chen, L. Jia, Y. Hou, H. Ji, H. Yang, T. Zhang, L. Liu, H.-J. Gao, T. A. Jung and Y. Wang, Quantum Spin Liquid Signatures in Monolayer 1T-NbSe2, *Nat. Commun.*, 2024, **15**(1), 2336, DOI: **10.1038/s41467-024-46612-1**.

27 R. Hiraoka, E. Minamitani, R. Arafune, N. Tsukahara, S. Watanabe, M. Kawai and N. Takagi, Single-Molecule Quantum Dot as a Kondo Simulator, *Nat. Commun.*, 2017, **8**(1), 16012, DOI: **10.1038/ncomms16012**.

28 M. Ternes, A. J. Heinrich and W.-D. Schneider, Spectroscopic Manifestations of the Kondo Effect on Single Adatoms, *J. Phys.: Condens. Matter*, 2009, **21**(5), 053001, DOI: **10.1088/0953-8984/21/5/053001**.

29 H. Okuyama, S. Kuwayama, Y. Nakazawa, S. Hatta and T. Aruga, Structure and Electronic States of Strongly Interacting Metal-Organic Interfaces: CuPc on Cu(100) and Cu(110), *Surf. Sci.*, 2022, **723**, 122126, DOI: **10.1016/j.susc.2022.122126**.

30 L. Garnier, B. Verlhac, P. Abufager, N. Lorente, M. Ormaza and L. Limot, The Kondo Effect of a Molecular Tip As a Magnetic Sensor, *Nano Lett.*, 2020, **20**(11), 8193–8199, DOI: **10.1021/acs.nanolett.0c03271**.

31 V. Madhavan, W. Chen, T. Jamneala, M. F. Crommie and N. S. Wingreen, Tunneling into a Single Magnetic Atom: Spectroscopic Evidence of the Kondo Resonance, *Science*, 1998, **280**(5363), 567–569, DOI: **10.1126/science.280.5363.567**.

32 J. Granet, M. Sicot, B. Kierren, S. Lamare, F. Chérioux, F. Baudelet, Y. Fagot-Revurat, L. Moreau and D. Malterre, Tuning the Kondo Resonance in Two-Dimensional Lattices of Cerium Molecular Complexes, *Nanoscale*, 2018, **10**(19), 9123–9132, DOI: **10.1039/C7NR08202A**.

33 C. G. Ayani, M. Pisarra, I. M. Ibarburu, M. Garnica, R. Miranda, F. Calleja, F. Martín and A. L. Vázquez De Parga, Probing the Phase Transition to a Coherent 2D Kondo Lattice, *Small*, 2023, 2303275, DOI: **10.1002/smll.202303275**.

34 L. Gao, W. Ji, Y. B. Hu, Z. H. Cheng, Z. T. Deng, Q. Liu, N. Jiang, X. Lin, W. Guo, S. X. Du, W. A. Hofer, X. C. Xie and H.-J. Gao, Site-Specific Kondo Effect at Ambient Temperatures in Iron-Based Molecules, *Phys. Rev. Lett.*, 2007, **99**(10), 106402, DOI: **10.1103/PhysRevLett.99.106402**.

35 Y.-S. Fu, Q.-K. Xue and R. Wiesendanger, Spin-Resolved Splitting of Kondo Resonances in the Presence of RKKY-Type Coupling, *Phys. Rev. Lett.*, 2012, **108**(8), 087203, DOI: **10.1103/PhysRevLett.108.087203**.

36 E. Minamitani, Y.-S. Fu, Q.-K. Xue, Y. Kim and S. Watanabe, Spatially Extended Underscreened Kondo State from Collective

Molecular Spin, *Phys. Rev. B:Condens. Matter Mater. Phys.*, 2015, **92**(7), 075144, DOI: 10.1103/PhysRevB.92.075144.

37 M. Garnica, F. Calleja, A. L. Vázquez De Parga and R. Miranda, Mapping Spin Distributions in Electron Acceptor Molecules Adsorbed on Nanostructured Graphene by the Kondo Effect, *Surf. Sci.*, 2014, **630**, 356–360, DOI: 10.1016/j.susc.2014.07.028.

38 L. Liu, K. Yang, Y. Jiang, B. Song, W. Xiao, S. Song, S. Du, M. Ouyang, W. A. Hofer, A. H. Castro Neto and H.-J. Gao, Revealing the Atomic Site-Dependent g Factor within a Single Magnetic Molecule via the Extended Kondo Effect, *Phys. Rev. Lett.*, 2015, **114**(12), 126601, DOI: 10.1103/PhysRevLett.114.126601.

39 L. She, Z. Shen, Z. Xie, L. Wang, Y. Song, X.-S. Wang, Y. Jia, Z. Zhang and W. Zhang, Magnetic Moment Preservation and Emergent Kondo Resonance of Co-Phthalocyanine on Semimetallic Sb(111), *Phys. Rev. Lett.*, 2022, **129**(2), 026802, DOI: 10.1103/PhysRevLett.129.026802.

40 I. Fernández-Torrente, K. J. Franke and J. I. Pascual, Vibrational Kondo Effect in Pure Organic Charge-Transfer Assemblies, *Phys. Rev. Lett.*, 2008, **101**(21), 217203, DOI: 10.1103/PhysRevLett.101.217203.

41 A. Mugarza, C. Krull, R. Robles, S. Stepanow, G. Ceballos and P. Gambardella, Spin Coupling and Relaxation inside Molecule–Metal Contacts, *Nat. Commun.*, 2011, **2**(1), 490, DOI: 10.1038/ncomms1497.

42 Kügel-et-al-2014-Relevance-of-Hybridization-and-Filling-of-3d-Orbitals-for-the-Kondo-Effect-in-Transition-Metal.Pdf.

43 A. Mugarza, C. Krull, R. Robles, S. Stepanow, G. Ceballos and P. Gambardella, Spin Coupling and Relaxation inside Molecule–Metal Contacts, *Nat. Commun.*, 2011, **2**, 490.

44 M. Moors, A. Krupski, S. Degen, M. Kralj, C. Becker and K. Wandelt, Scanning Tunneling Microscopy and Spectroscopy Investigations of Copper Phthalocyanine Adsorbed on Al2O3/Ni3Al(111), *Appl. Surf. Sci.*, 2008, **254**(14), 4251–4257, DOI: 10.1016/j.apsusc.2008.01.029.

45 F. Donati, S. Rusponi, S. Stepanow, C. Wäckerlin, A. Singha, L. Persichetti, R. Baltic, K. Diller, F. Patthey, E. Fernandes, J. Dreiser, Ž. Šljivančanin, K. Kummer, C. Nistor, P. Gambardella and H. Brune, Magnetic Remanence in Single Atoms, *Science*, 2016, **352**(6283), 318–321, DOI: 10.1126/science.aad9898.

46 T.-C. Hung, B. Kiraly, J. H. Strik, A. A. Khajetoorians and D. Wegner, Plasmon-Driven Motion of an Individual Molecule, *Nano Lett.*, 2021, **21**(12), 5006–5012, DOI: 10.1021/acs.nanolett.1c00788.

47 K. A. Cochrane, T. S. Roussy, B. Yuan, G. Tom, E. Mårsell and S. A. Burke, Molecularly Resolved Electronic Landscapes of Differing Acceptor–Donor Interface Geometries, *J. Phys. Chem. C*, 2018, **122**(15), 8437–8444, DOI: 10.1021/acs.jpcc.8b01396.

48 T. Miyamachi, M. Gruber, V. Davesne, M. Bowen, S. Boukari, L. Joly, F. Scheurer, G. Rogez, T. K. Yamada, P. Ohresser, E. Beaurepaire and W. Wulfhekel, Robust Spin Crossover and Memristance across a Single Molecule, *Nat. Commun.*, 2012, **3**(1), 938, DOI: 10.1038/ncomms1940.

49 S. S. P. Parkin, C. Kaiser, A. Panchula, P. M. Rice, B. Hughes, M. Samant and S.-H. Yang, Giant Tunnelling Magnetoresistance at Room Temperature with MgO (100) Tunnel Barriers, *Nat. Mater.*, 2004, **3**(12), 862–867, DOI: 10.1038/nmat1256.

50 S. Yuasa, T. Nagahama, A. Fukushima, Y. Suzuki and K. Ando, Giant Room-Temperature Magnetoresistance in Single-Crystal Fe/MgO/Fe Magnetic Tunnel Junctions, *Nat. Mater.*, 2004, **3**(12), 868–871, DOI: 10.1038/nmat1257.

51 S. Yuasa, A. Fukushima, T. Nagahama, K. Ando and Y. Suzuki, High Tunnel Magnetoresistance at Room Temperature in Fully Epitaxial Fe/MgO/Fe Tunnel Junctions Due to Coherent Spin-Polarized Tunneling, *Jpn. J. Appl. Phys.*, 2004, **43**(4B), L588, DOI: 10.1143/JJAP.43.L588.

52 S. Schmaus, A. Bagrets, Y. Nahas, T. K. Yamada, A. Bork, M. Bowen, E. Beaurepaire, F. Evers and W. Wulfhekel, Giant Magnetoresistance through a Single Molecule, *Nat. Nanotechnol.*, 2011, **6**(3), 185–189, DOI: 10.1038/nnano.2011.11.

53 A. Bagrets, S. Schmaus, A. Jaafar, D. Kramczynski, T. K. Yamada, M. Alouani, W. Wulfhekel and F. Evers, Single Molecule Magnetoresistance with Combined Antiferromagnetic and Ferromagnetic Electrodes, *Nano Lett.*, 2012, **12**(10), 5131–5136, DOI: 10.1021/nl301967t.

54 T. K. Yamada, Y. Yamagishi, S. Nakashima, Y. Kitaoka and K. Nakamura, Role of π–d Hybridization in a 300-K Organic-Magnetic Interface: Metal-Free Phthalocyanine Single Molecules on a Bcc Fe(001) Whisker, *Phys. Rev. B*, 2016, **94**(19), 195437, DOI: 10.1103/PhysRevB.94.195437.

55 N. K. M. Nazriq, P. Krüger and T. Kazu Yamada, Improving MgO/Fe Insulator-Metal Interface Structure through Oxygen-Precoating of Fe(0 0 1), *Appl. Surf. Sci.*, 2023, **618**, 156628, DOI: 10.1016/j.apsusc.2023.156628.

56 T. K. Yamada, Y. Sakaguchi, L. Gerhard and W. Wulfhekel, Temperature Control of the Growth of Iron Oxide Nanoislands on Fe(001), *Jpn. J. Appl. Phys.*, 2016, **55**(8S1), 08NB14, DOI: 10.7567/JJAP.55.08NB14.

57 T. K. Yamada and A. L. Vazquez de Parga, Room Temperature Spin-Polarizations of Mn-Based Antiferromagnetic Nanoelectrodes, *Appl. Phys. Lett.*, 2014, **105**(18), 183109, DOI: 10.1063/1.4901047.

58 N. K. M. Nazriq, P. Krüger and T. K. Yamada, Carbon Monoxide Stripe Motion Driven by Correlated Lateral Hopping in a 1.4 × 1.4 Monolayer Phase on Cu(111), *J. Phys. Chem. Lett.*, 2020, **11**(5), 1753–1761, DOI: 10.1021/acs.jpclett.9b03645.

59 N. K. M. Nazriq, E. Minamitani and T. K. Yamada, CO-Tip Manipulation Using Repulsive Interactions, *Nanotechnology*, 2018, **29**(49), 495701, DOI: 10.1088/1361-6528/aae0df.

60 T. K. Yamada, R. Nemoto, F. Nishino, T. Hosokai, C.-H. Wang, M. Horie, Y. Hasegawa, S. Kera and P. Krüger, On-Surface Growth of Transition-Metal Cobalt Nanoclusters Using a 2D Crown-Ether Array, *J. Mater. Chem. C*, 2024, **128**(3), 1477–1486, DOI: 10.1039/D3TC03339B.

61 R. Nemoto, P. Krüger, A. N. Putri Hartini, T. Hosokai, M. Horie, S. Kera and T. K. Yamada, Well-Ordered Monolayer Growth of Crown-Ether Ring Molecules on Cu(111) in

Ultra-High Vacuum: An STM, UPS, and DFT Study, *J. Phys. Chem. C*, 2019, **123**(31), 18939–18950, DOI: **10.1021/acs.jpcc.9b03335**.

62 C. G. Ayani, F. Calleja, I. M. Ibarburu, P. Casado Aguilar, N. K. M. Nazriq, T. K. Yamada, M. Garnica, A. L. Vázquez De Parga and R. Miranda, Switchable Molecular Functionalization of an STM Tip: From a Yu–Shiba–Rusinov Tip to a Kondo Tip, *Nanoscale*, 2022, **14**(40), 15111–15118, DOI: **10.1039/D1NR08227B**.

63 T. Yamaguchi, E. Inami, Y. Goto, Y. Sakai, S. Sasaki, T. Ohno and T. K. Yamada, Fabrication of Tungsten Tip Probes within 3 s by Using Flame Etching, *Rev. Sci. Instrum.*, 2019, **90**(6), 063701, DOI: **10.1063/1.5085251**.

64 Y. Goto, R. Suizu, Y. Noguchi and T. K. Yamada, Oxidative Vaporization Etching for Molybdenum Tip Formation in Air, *Appl. Surf. Sci.*, 2021, **542**, 148642, DOI: **10.1016/j.apsusc.2020.148642**.

65 T. K. Yamada, T. Abe, N. M. K. Nazriq and T. Irisawa, Electron-Bombarded ⟨110⟩-Oriented Tungsten Tips for Stable Tunneling Electron Emission, *Rev. Sci. Instrum.*, 2016, **87**(3), 033703, DOI: **10.1063/1.4943074**.

66 I. Horcas, R. Fernández, J. M. Gómez-Rodríguez, J. Colchero, J. Gómez-Herrero and A. M. Baro, WSXM: A Software for Scanning Probe Microscopy and a Tool for Nanotechnology, *Rev. Sci. Instrum.*, 2007, **78**(1), 013705, DOI: **10.1063/1.2432410**.

67 U. Fano, Effects of Configuration Interaction on Intensities and Phase Shifts, *Phys. Rev.*, 1961, **124**(6), 1866–1878, DOI: **10.1103/PhysRev.124.1866**.

68 A. E. Miroshnichenko, S. Flach and Y. S. Kivshar, Fano Resonances in Nanoscale Structures, *Rev. Mod. Phys.*, 2010, **82**(3), 2257–2298, DOI: **10.1103/RevModPhys.82.2257**.

69 K. Nagaoka, T. Jamneala, M. Grobis and M. F. Crommie, Temperature Dependence of a Single Kondo Impurity, *Phys. Rev. Lett.*, 2002, **88**(7), 077205, DOI: **10.1103/PhysRevLett.88.077205**.

70 G. Binnig, H. Rohrer, C. Gerber and E. Weibel, Surface Studies by Scanning Tunneling Microscopy, *Phys. Rev. Lett.*, 1982, **49**(1), 57–61, DOI: **10.1103/PhysRevLett.49.57**.

71 J. Tersoff and D. R. Hamann, Theory of the Scanning Tunneling Microscope, *Phys. Rev. B:Condens. Matter Mater. Phys.*, 1985, **31**(2), 805–813, DOI: **10.1103/PhysRevB.31.805**.

72 V. A. Ukraintsev, Data Evaluation Technique for Electron-Tunneling Spectroscopy, *Phys. Rev. B:Condens. Matter Mater. Phys.*, 1996, **53**(16), 11176–11185, DOI: **10.1103/PhysRevB.53.11176**.

73 T. K. Yamada, H. Tamura, M. Shishido, T. Irisawa and T. Mizoguchi, Surface Reconstruction of Clean Bcc-Fe{110}: A Quasi-Hexagonal Top-Layer with Periodic Height Modulation, *Surf. Sci.*, 2009, **603**(2), 315–319, DOI: **10.1016/j.susc.2008.11.010**.

74 J. A. Stroscio, D. T. Pierce, A. Davies, R. J. Celotta and M. Weinert, Tunneling Spectroscopy of Bcc (001) Surface States, *Phys. Rev. Lett.*, 1995, **75**(16), 2960–2963, DOI: **10.1103/PhysRevLett.75.2960**.

75 T. K. Yamada, M. M. J. Bischoff, G. M. M. Heijnen, T. Mizoguchi and H. van Kempen, Observation of Spin-Polarized Surface States on Ultrathin Bct Mn(001) Films by Spin-Polarized Scanning Tunneling Spectroscopy, *Phys. Rev. Lett.*, 2003, **90**(5), 056803, DOI: **10.1103/PhysRevLett.90.056803**.

76 Y. Kosuge and T. K. Yamada, Spin-Polarized Scanning Tunneling Microscopy Study of Non-Collinear Magnetic Coupling in Layerwise Antiferromagnetic Mn(001) Ultra-Thin Films on Fe(001) due to Interface Roughening, *Vac. Surf. Sci.*, 2020, **63**(9), 459–464, DOI: **10.1380/vss.63.459**.

77 U. Schlickum, N. Janke-Gilman, W. Wulfhekel and J. Kirschner, Step-Induced Frustration of Antiferromagnetic Order in Mn on Fe(001), *Phys. Rev. Lett.*, 2004, **92**(10), 107203, DOI: **10.1103/PhysRevLett.92.107203**.

78 A. Cattoni, D. Petti, S. Brivio, M. Cantoni, R. Bertacco and F. Ciccacci, MgO/Fe(001) and MgO/Fe(001)–p(1 × 1) O Interfaces for Magnetic Tunnel Junctions: A Comparative Study, *Phys. Rev. B:Condens. Matter Mater. Phys.*, 2009, **80**(10), 104437, DOI: **10.1103/PhysRevB.80.104437**.

79 F. Donati, P. Sessi, S. Achilli, A. Li Bassi, M. Passoni, C. S. Casari, C. E. Bottani, A. Brambilla, A. Picone, M. Finazzi, L. Duò, M. I. Trioni and F. Ciccacci, Scanning Tunneling Spectroscopy of the Fe(001)–p(1 × 1) O Surface, *Phys. Rev. B:Condens. Matter Mater. Phys.*, 2009, **79**(19), 195430, DOI: **10.1103/PhysRevB.79.195430**.

80 N. K. M. Nazriq, P. Krüger and T. Kazu Yamada, Improving MgO/Fe Insulator-Metal Interface Structure through Oxygen-Precoating of Fe(0 0 1), *Appl. Surf. Sci.*, 2023, **618**, 156628, DOI: **10.1016/j.apsusc.2023.156628**.

81 E. Inami, M. Yamaguchi, T. Yamaguchi, M. Shimasaki and T. K. Yamada, Controlled Deposition Number of Organic Molecules Using Quartz Crystal Microbalance Evaluated by Scanning Tunneling Microscopy Single-Molecule-Counting, *Anal. Chem.*, 2018, **90**(15), 8954–8959, DOI: **10.1021/acs.analchem.8b01118**.

82 G. Kresse and D. Joubert, From Ultrasoft Pseudopotentials to the Projector Augmented-Wave Method, *Phys. Rev. B:Condens. Matter Mater. Phys.*, 1999, **59**(3), 1758–1775, DOI: **10.1103/PhysRevB.59.1758**.

83 G. Kresse and J. Furthmüller, Efficient Iterative Schemes for *Ab Initio* Total-Energy Calculations Using a Plane-Wave Basis Set, *Phys. Rev. B:Condens. Matter Mater. Phys.*, 1996, **54**(16), 11169–11186, DOI: **10.1103/PhysRevB.54.11169**.

84 J. Heyd, G. E. Scuseria and M. Ernzerhof, Hybrid Functionals Based on a Screened Coulomb Potential, *J. Chem. Phys.*, 2003, **118**(18), 8207–8215, DOI: **10.1063/1.1564060**.

85 A. V. Krukau, O. A. Vydrov, A. F. Izmaylov and G. E. Scuseria, Influence of the Exchange Screening Parameter on the Performance of Screened Hybrid Functionals, *J. Chem. Phys.*, 2006, **125**(22), 224106, DOI: **10.1063/1.2404663**.

86 N. Marom, O. Hod, G. E. Scuseria and L. Kronik, Electronic Structure of Copper Phthalocyanine: A Comparative Density Functional Theory Study, *J. Chem. Phys.*, 2008, **128**(16), 164107, DOI: **10.1063/1.2898540**.

87 K. Miwa, H. Imada, S. Kawahara and Y. Kim, Effects of Molecule-Insulator Interaction on Geometric Property of a Single Phthalocyanine Molecule Adsorbed on an Ultrathin

NaCl Film, *Phys. Rev. B*, 2016, **93**(16), 165419, DOI: **10.1103/PhysRevB.93.165419**.

88 I. V. Borzenets, J. Shim, J. C. H. Chen, A. Ludwig, A. D. Wieck, S. Tarucha, H.-S. Sim and M. Yamamoto, Observation of the Kondo Screening Cloud, *Nature*, 2020, **579**(7798), 210–213, DOI: **10.1038/s41586-020-2058-6**.

89 D. O. Bang, T. Nozaki, Y. Suzuki, K. Rhie, T.-S. Kim, A. Fukushima, S. Yuasa, E. Minamitani, H. Nakanishi and H. Kasai, Study of Kondo Effect in MgO-Based Magnetic Tunnel Junctions by Electron Tunnelling Spectroscopy, *J. Phys.:Conf. Ser.*, 2010, **200**(5), 052004, DOI: **10.1088/1742-6596/200/5/052004**.

90 S. Baumann, F. Donati, S. Stepanow, S. Rusponi, W. Paul, S. Gangopadhyay, I. G. Rau, G. E. Pacchioni, L. Gragnaniello, M. Pivetta, J. Dreiser, C. Piamonteze, C. P. Lutz, R. M. Macfarlane, B. A. Jones, P. Gambardella, A. J. Heinrich and H. Brune, Origin of Perpendicular Magnetic Anisotropy and Large Orbital Moment in Fe Atoms on MgO, *Phys. Rev. Lett.*, 2015, **115**(23), 237202, DOI: **10.1103/PhysRevLett.115.237202**.

91 T. Katayama, S. Yuasa, J. Velev, M. Y. Zhuravlev, S. S. Jaswal and E. Y. Tsymbal, Interlayer Exchange Coupling in Fe/MgO/Fe Magnetic Tunnel Junctions, *Appl. Phys. Lett.*, 2006, **89**(11), 112503, DOI: **10.1063/1.2349321**.

92 H. X. Yang, M. Chshiev, A. Kalitsov, A. Schuhl and W. H. Butler, Effect of Structural Relaxation and Oxidation Conditions on Interlayer Exchange Coupling in Fe|MgO|Fe Tunnel Junctions, *Appl. Phys. Lett.*, 2010, **96**(26), 262509, DOI: **10.1063/1.3459148**.

93 X. Zhang, C. Wolf, Y. Wang, H. Aubin, T. Bilgeri, P. Willke, A. J. Heinrich and T. Choi, Electron Spin Resonance of Single Iron Phthalocyanine Molecules and Role of Their Non-Localized Spins in Magnetic Interactions, *Nat. Chem.*, 2022, **14**(1), 59–65, DOI: **10.1038/s41557-021-00827-7**.

94 R. Kawaguchi, K. Hashimoto, T. Kakudate, K. Katoh, M. Yamashita and T. Komeda, Spatially Resolving Electron Spin Resonance of π-Radical in Single-Molecule Magnet, *Nano Lett.*, 2023, **23**(1), 213–219, DOI: **10.1021/acs.nanolett.2c04049**.

95 F. Delgado and N. Lorente, A Theoretical Review on the Single-Impurity Electron Spin Resonance on Surfaces, *Prog. Surf. Sci.*, 2021, **96**(2), 100625, DOI: **10.1016/j.progsurf.2021.100625**.

96 M. Mannini, F. Pineider, P. Sainctavit, L. Joly, A. Fraile-Rodríguez, M.-A. Arrio, C. Cartier dit Moulin, W. Wernsdorfer, A. Cornia, D. Gatteschi and R. Sessoli, X-Ray Magnetic Circular Dichroism Picks out Single-Molecule Magnets Suitable for Nanodevices, *Adv. Mater.*, 2009, **21**(2), 167–171, DOI: **10.1002/adma.200801883**.

97 C. Wäckerlin, A. Cahlík, J. Goikoetxea, O. Stetsovych, D. Medvedeva, J. Redondo, M. Švec, B. Delley, M. Ondráček, A. Pinar, M. Blanco-Rey, J. Kolorenč, A. Arnau and P. Jelínek, Role of the Magnetic Anisotropy in Atomic-Spin Sensing of 1D Molecular Chains, *ACS Nano*, 2022, **16**(10), 16402–16413, DOI: **10.1021/acsnano.2c05609**.

98 A.-A. Haghighirad, R. Ichikawa, T. Miyamachi, H. Ishii, S. Akamatsu, E. Masui, O. Ishiyama, H. Iwayama, E. Nakamura, T. Yokoyama, E. Inami and T. K. Yamada, STM Imaging and Electronic Correlation in van der Waals Ferromagnet Fe_3 $GeTe_2$, *Jpn. J. Appl. Phys.*, 2025, **64**(4), 040805, DOI: **10.35848/1347-4065/adc7be**.

